ACS Sustainable Chemistry & Engineering

Research Article

pubs.acs.org/journal/ascecg

# Synthesis and Characterization of *O*-Alkylated Amidium Ionic Liquids

Zheng Jian Chen,[†] Hong Wei Xi,[†] Kok Hwa Lim,[†,‡] and Jong-Min Lee*,[†]

[†]School of Chemical and Biomedical Engineering, Nanyang Technological University, 62 Nanyang Drive, Singapore 637459, Singapore

[‡]Singapore Institute of Technology, 10 Dover Drive, Singapore 138683, Singapore

**ABSTRACT:** In the present study, a new series of ionic liquids (ILs) derived from low-cost amides and lactams (cyclic amides), such as *N*,*N*-dimethylformamide (DMF), were synthesized and characterized. Unlike other nucleophiles like amines, the alkylation reaction of the amides with alkyl triflates to form cationic species takes place at the carbonyl oxygen atom, instead of the nitrogen atom. For these *O*-alkylated amidium ILs, the basic physicochemical properties, such as melting point, glass transition temperature, plastic crystal phase transition, thermal stability, density, surface tension, viscosity, ionic conductivity and electrochemical window, were investigated and studied. Generally, these ILs are distinguished by low viscosity and high conductivity, in particular the DMF-derived ILs with viscosity as low as 21.6 cP and conductivity up to 15.45 mS $cm^{-1}$ at 25 °C. This result should be attributed to the cationic DMF structures: planar geometry, low symmetry, C2-proton and ether moiety, resulting in much lower viscosity and higher conductivity than the best-known imidazolium ILs. Meanwhile, these amidium ILs also possess wide electrochemical windows (~4.5 V) comparable to imidazolium ILs, implying their potential in electrochemical applications. Furthermore, several of the amidium ILs can form plastic crystal with a maximum enthalpy gain of −35.7 J $g^{-1}$ at the temperature range of −10−90 °C.

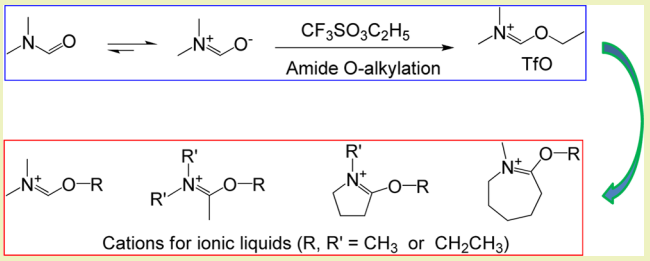


**KEYWORDS:** *Amide, O-alkylation, physicochemical property, plastic crystal, viscosity, conductivity*

## INTRODUCTION

Ionic liquids (ILs), a special class of molten salts, are composed solely of ions and nevertheless are liquid near room temperature. Due to their entire ionic composition, ILs are unique in a set of characters, such as negligible vapor pressure, low flammability, wide liquid temperature range, high ionic conductivity, intrinsic electrostatic field, extra solvency, and so on.[1,2] These characters enable them to serve as a superior and environmentally friendly alternative to the conventional organic solvents.[3,4] Furthermore, ILs have emerged as a versatile platform for a wide variety of fundamental research and practical applications, such as organic synthesis,[5] enzyme catalysis,[6] biomass processing,[7] gas capture,[8] carbon precursor,[9] nanotech,[10] energy storage,[11] electrochemical devices,[12] nuclear fuel cycle,[13] hypergolic fluids,[14] lubricants,[15] magnetic fluids,[16] optical materials,[17] and many more.

However, the topic of ILs is currently restricted to academic research, rather than to industrial applications. There are several barriers to the large-scale use of ILs. First of all, ILs cannot be recycled by simple distillation like organic solvents, because of their very low vapor pressure.[18] On this account, many efforts have been made to study such low vapor pressure, as well as to develop "distillable" ILs.[19−27] Earle et al.[22] achieved the vacuum distillation of ILs without decomposition by vaporization of the neutral ion clusters at elevated temperatures. Yet this distillation process is too slow to be practically applied,[23] e.g., 0.12 g $h^{-1}$ for [EMIm]$NTf_2$ at 300 °C and 0.1 mbar.[22] Recent studies indicated that protic ILs can be readily converted back to organic acid and base precursors via proton transfer at high temperatures.[24−27] By vacuum distillation of the regenerated precursors, King et al.[25] recovered the acid−base conjugate ILs that were used to dissolve cellulose, with recovery up to 99.4%. Second, ILs are usually highly viscous, due to the strong interion Coulomb interactions. High viscosity may cause severe limitations in use, such as low conductivity, low mass transfer rate, poor wettability, as well as operational problems like infiltration.[28] Lastly, but not least, the current price of ILs is still too high for large-scale use. But we believe that the price will continuously drop with the increase of demand and the development of low-cost ILs.

Recently, cheap amides have been used as building blocks to form ILs, such as deep eutectic,[29,30] protic,[31−38] and aprotic[39,40] types. These amide derivatives could be tailor-made for various applications, such as $CO_2$ dissolution,[31,32] electrolytes,[33−35,39] esterification catalysis,[36] ionothermal carbonization of sugar,[37] extraction of metal ions,[38] liquid crystal,[40] and so on. Generally, most ILs are prepared through alkylation/quaternization at the electron-rich N, P, or S atom position like in 1-methylimidazole.[41] Whereas in amides, the nitrogen atom is conjugated to an electron-withdrawing carbonyl group, and thus the lone pair electrons in nitrogen atom tend to delocalize into the carbonyl

Received: November 19, 2014
Revised: January 4, 2015
Published: January 20, 2015





DOI: 10.1021/sc5007347
ACS Sustainable Chem. Eng. 2015, 3, 325−333

oxygen atom, resulting in making the N atom less nucleophilic and the O atom more nucleophilic.[42] Consequently, the amide alkylation is more likely to occur at O than N. Though the amide *O*-alkylation was proposed in 1956,[43] and later confirmed elsewhere,[35,37,38,44−46] the paradoxical mechanism of *N*-alkylation was still employed until very recently.[33,34,39,40]

In our recent work,[47] the amide *O*-alkylation was found to be readily reversible with temperature, and the amidium ILs are "distillable" by vacuum evaporation of the regenerated volatile precursors at high temperatures. In this study, 24 *O*-alkylated amidium ILs were prepared and characterized to systematically study their properties and potential applications.

## RESULTS AND DISCUSSION

The synthetic route of the *O*-alkylated amidium ILs is typically shown in Scheme 1 (see the Experimental Section for details).

**Scheme 1. Typical Synthetic Route of Amidium ILs (upper), and the Structures and Abbreviations of Cations and Anions Used in This Study**

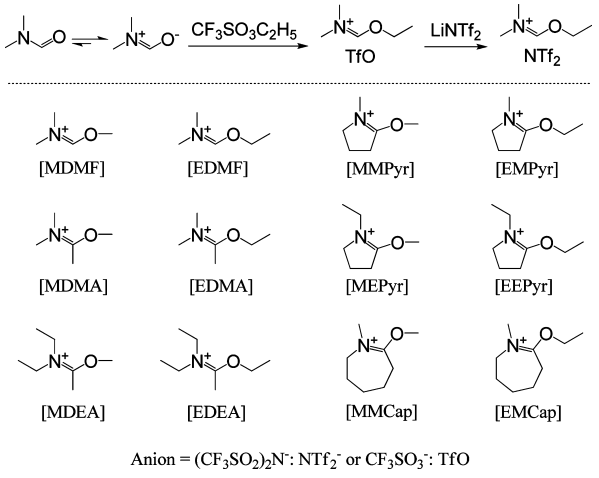


Anion = $(CF_3SO_2)_2N^-$: $NTf_2^-$ or $CF_3SO_3^-$: TfO

The reaction of amides with alkyl triflates takes place at the O atom instead of the N atom, as a result of the electron delocalization in amides.[47] In total, six amides [*N*,*N*-dimethylformamide (DMF), *N*,*N*-dimethylacetamide (DMA), *N*,*N*-diethylacetamide (DEA), *N*-methylpyrrolidone (MPyr), *N*-ethylpyrrolidone (EPyr), and *N*-methylcaprolactam (MCap)], and two alkylating agents (methyl and ethyl triflates) were utilized for synthesis of 12 TfO-based amidium ILs. Moreover, $NTf_2$-based ILs were also prepared by anion exchange.

The structures of the amidium ILs were identified by $^1H/^{13}C$ NMR spectra (see the Experimental Section for details). As shown in Figure 1, the experimental NMR signals match very well with the proposed structure. In both $^1H$ and $^{13}C$ NMR spectra, the signals assigned to the two methyl groups in $=N^+(CH_3)_2$ do not coalesce with a clear separation, which agrees exactly with the asymmetry caused by the C═N double bond in the *O*-ethylated case. If in the *N*-ethylated case, the two signals would coalesce into a singlet. The proton in $N^+$═C(H)—O appears at a high $^1H$ chemical shift of 8.35 ppm, and the carbon also resonates at a high $^{13}C$ chemical shift of 166.84 ppm, according with the conjugated system. The quartet (127.41, 123.16, 118.92, 114.67 ppm) split by fluorine in $^{13}C$ NMR assigned to trifluoromethyl group ($CF_3$) identifies the presence of TfO anion.

The fundamental physicochemical properties of the amidium ILs were investigated and studied, including thermal stability ($T_d$), liquid−solid phase transition, density ($\rho$), surface tension ($\gamma$), viscosity ($\eta$) and its activation energy ($\Delta H_\eta$), conductivity ($\kappa$), and electrochemical stability window (EW), as summarized in Tables 1 and 2. For the purpose of comparison, two 1-ethyl-3-methylimidazolium [EMIm] based ILs, which are one of the best-known ILs with excellent performance, were also characterized.

The liquid−solid phase transition behaviors of the amidium ILs were examined using differential scanning calorimetry (DSC) upon a cooling and heating cycle at a scanning rate of 5 K $min^{-1}$. The corresponding values for glass-transition temperature ($T_g$), crystallization temperature ($T_c$), melting point ($T_m$), solid-plastic transition temperature ($T_{s\text{-}p}$ and $T_{p\text{-}s}$), and the enthalpy change ($\Delta H$) are summarized in Table 1. Generally, four types of phase transition processes were

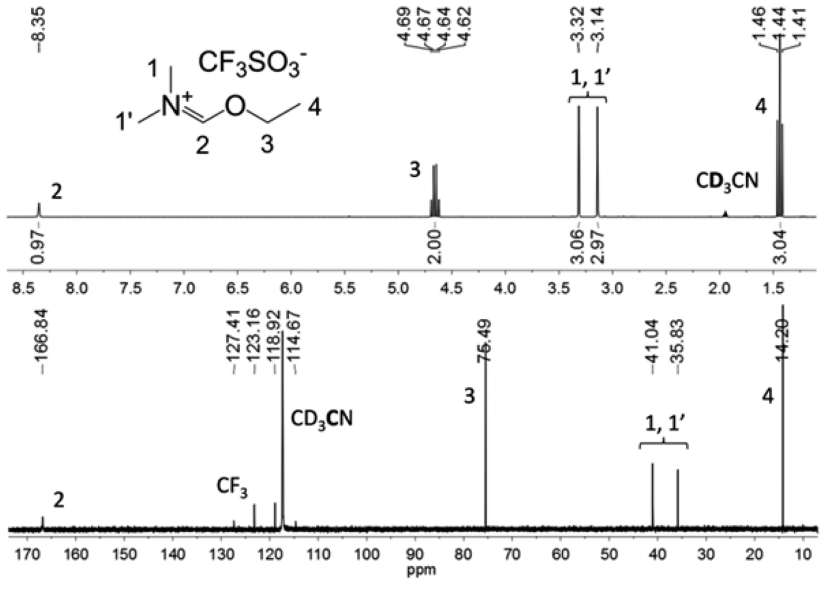


**Figure 1.** $^1H/^{13}C$ NMR of [EDMF]TfO in $CD_3CN$.


DOI: 10.1021/sc5007347
ACS Sustainable Chem. Eng. 2015, 3, 325−333

**Table 1. Phase Transition Properties and Thermal Stabilities of the Amidium ILs**

| entry | IL | $T_g$[a] (°C) | $T_{s\text{-}p}$[b] (°C) | $\Delta H_{s\text{-}p}$[c] (J g$^{-1}$) | $T_m$[d] (°C) | $\Delta H_m$[e] (J g$^{-1}$) | $T_c$[f] (°C) | $\Delta H_c$[g] (J g$^{-1}$) | $T_{p\text{-}s}$[h] (°C) | $\Delta H_{p\text{-}s}$[i] (J g$^{-1}$) | $T_d$[j] (°C) |
|---|---|---|---|---|---|---|---|---|---|---|---|
| 1 | [MDMF]TfO | | | | 23.2 | −37.6 | −6.95 | 34.9 | | | 165 |
| 2 | [EDMF]TfO | −100.5 | | | −32.5 | −40.7 | (−64.0) | 43.3 | | | 165 |
| 3 | [MDMA]TfO | | | | 42.5 | −34.9 | 24.6 | 34.3 | | | 184 |
| 4 | [EDMA]TfO | | | | 77.0 | −72.2 | 61.8 | 74.1 | | | 165 |
| 5 | [MDEA]TfO | | | | 41.0 | −55.1 | 13.2 | 38.1 | −11.1 | 12.0 | 179 |
| 6 | [EDEA]TfO | | 28.1 | −35.7 | 48.5 | −34.4 | 14.5 | 67.5 | 6.5 | 4.7 | 177 |
| 7 | [MMPyr]TfO | | | | 97.6 | −73.2 | 58.9 | 74.5 | | | 184 |
| 8 | [EMPyr]TfO | | | | 42.1 | −67.6 | 15.3 | 66.4 | | | 166 |
| 9 | [MEPyr]TfO | | | | 14.7 | −28.0 | −27.4 | 28.5 | | | 177 |
| 10 | [EEPyr]TfO | | | | 34.1 | −44.6 | 4.8 | 49.2 | | | 171 |
| 11 | [MMCap]TfO | | | | 33.5 | −26.1 | 9.4 | 28.8 | | | 176 |
| 12 | [EMCap]TfO | | | | 40.1 | −52.1 | 0.0 | 51.1 | | | 164 |
| 13 | [MDMF]$NTf_2$ | | | | 37.6 | −52.2 | −16.1 | 45.0 | | | 171 |
| 14 | [EDMF]$NTf_2$ | −91.6 | | | 2.9 | −50.7 | (−60.7) | 36.3 | | | 196 |
| 15 | [MDMA]$NTf_2$ | | 31.6 | −17.4 | 77.2 | −28.8 | 67.1 | 28.5 | 24.6 | 18.1 | 192 |
| 16 | [EDMA]$NTf_2$ | | | | 33.1 | −46.5 | 11.3 | 30.7 | 6.1 | 13.9 | 199 |
| 17 | [MDEA]$NTf_2$ | | | | 28.3 | −48.1 | 4.0 | 45.8 | | | 192 |
| 18 | [EDEA]$NTf_2$ | | | | 53.8 | −75.3 | 21.9 | 68.7 | | | 202 |
| 19 | [MMPyr]$NTf_2$ | | 52.6 | −12.8 | 89.6 | −29.5 | 87.2 | 29.5 | 49.5 | 13.5 | 179 |
| 20 | [EMPyr]$NTf_2$ | | 33.5 | −21.3 | 38.4 | −46.3 | 30.4 | 20.6 | 21.4 | 23.2 | 198 |
| 21 | [MEPyr]$NTf_2$ | | | | 39.4 | −65.9 | 15.6 | 20.1 | −2.0 | 33.3 | 179 |
| 22 | [EEPyr]$NTf_2$ | | | | 29.0 | −55.0 | 10.0 | 53.7 | | | 204 |
| 23 | [MMCap]$NTf_2$ | | 37.5 | −19.2 | 67.6 | −24.7 | 62.8 | 26.5 | 32.9 | 19.6 | 175 |
| 24 | [EMCap]$NTf_2$ | | | | 44.4 | −44.2 | 42.3 | 22.2 | 35.6 | 21.3 | 199 |

[a]Glass transition temperature. [b]Solid-plastic crystal transition temperature upon heating. [c]Enthalpy of solid-plastic crystal transition upon heating. [d]Melting point. [e]Enthalpy of melting. [f]Crystallization temperature (cold crystallization). [g]Enthalpy of crystallization. [h]Plastic crystal-solid transition temperature upon cooling. [i]Enthalpy of plastic crystal-solid transition upon cooling. [j]Thermal decomposition temperature at 5% weight loss.

**Table 2. Basic Properties of the Amidium and [EMIm] ILs**

| entry | IL | $\rho$[a] (g cm$^{-3}$) | $\gamma$[b] (mN m$^{-1}$) | $\eta_{25}$[c] (cP) | $\eta_{50}$[d] (cP) | $\Delta H_\eta$[e] (kJ mol$^{-1}$) | $\kappa$[f] (mS cm$^{-1}$) | $E_{cathodic}$[g] (V) | $E_{anodic}$[h] (V) | EW[i] (V) |
|---|---|---|---|---|---|---|---|---|---|---|
| 1 | [MDMF]TfO | 1.4126 | 41.3 | 29.7 | 13.1 | 24.66 | 15.45 | −1.62 | 2.82 | 4.44 |
| 2 | [EDMF]TfO | 1.3492 | 35.8 | 22.4 | 10.8 | 22.62 | 14.46 | −1.61 | 2.80 | 4.41 |
| 3 | [MDEA]TfO | | | | 42.8 | | | | | |
| 4 | [EDEA]TfO | | | | 31.5 | | | | | |
| 5 | [EMPyr]TfO | | | | 22.9 | | | | | |
| 6 | [MEPyr]TfO | 1.3675 | 40.1 | 85.1 | 29.5 | 32.39 | 4.83 | −1.87 | 2.80 | 4.67 |
| 7 | [EEPyr]TfO | 1.3165 | 35.1 | 52.3 | 20.6 | 29.19 | 6.15 | −1.85 | 2.77 | 4.62 |
| 8 | [EMCap]TfO | | | | 58.5 | | | | | |
| 9 | [MDMF]$NTf_2$ | 1.5405 | 36.2 | 29.3 | 12.8 | 23.68 | 10.96 | −1.60 | 2.81 | 4.41 |
| 10 | [EDMF]$NTf_2$ | 1.4946 | 34.9 | 21.6 | 10.2 | 21.53 | 11.29 | −1.61 | 2.86 | 4.47 |
| 11 | [EDMA]$NTf_2$ | 1.4688 | 34.5 | 40.8 | 16.7 | 26.17 | 6.59 | −1.83 | 2.81 | 4.64 |
| 12 | [MDEA]$NTf_2$ | 1.4469 | 35.1 | 66.9 | 24.1 | 30.01 | 3.48 | −1.81 | 2.82 | 4.63 |
| 13 | [EDEA]$NTf_2$ | | | 54.9 | 20.7 | 28.51 | | | | |
| 14 | [EMPyr]$NTf_2$ | | | | 16.7 | | | | | |
| 15 | [MEPyr]$NTf_2$ | | | 46.2 | 19.0 | 26.31 | | | | |
| 16 | [EEPyr]$NTf_2$ | 1.4460 | 35.1 | 33.7 | 14.6 | 25.04 | 6.10 | −1.88 | 2.74 | 4.62 |
| 17 | [EMCap]$NTf_2$ | | | | 26.9 | | | | | |
| 18 | [EMIm]TfO | 1.3850 | 41.9 | 43.6 | 17.4 | 26.36 | 9.27 | −2.19 | 2.26 | 4.45 |
| 19 | [EMIm]$NTf_2$ | 1.5182 | 39.0 | 32.0 | 13.9 | 24.42 | 8.96 | −2.18 | 2.38 | 4.56 |

[a]Density at 25.0 °C. [b]Surface tension at 25.0 °C. [c]Viscosity at 25.0 °C. [d]Viscosity at 50.0 °C. [e]Activation energy of viscosity. [f]Conductivity at 25.0 °C. [g]Cathodic potential limit. [h]Anodic potential limit. [i]Electrochemical windows.

observed from the DSC measurements, as depicted in Figure 2. The first type of process consists of simple crystallization and melting, upon cooling and heating, respectively (Figure 2a, entries 1, 3, 4, 7−13, 17, 18, and 22 in Table 1). The samples in this case are very prone to form an ordered crystal, which prevents the appearance of the second-order phase transition, such as glass transition. For the second type, the involved samples display glass transition before cold crystallization and melting point (Figure 2b, entries 2 and 14 in Table 1). The two ILs engaging in this type are both based on the [EDMF] cation. An argument can be made that [EDMF]-based ILs are more inclined to be amorphous glass rather than ordered solid upon cooling. And, actually the two ILs based on [EDMF] have the lower melting points than the others, for a given anion. The third type is characteristic of two solid states upon both cooling and heating (Figure 2c, entries 6, 15, 19, 20, and 23 in Table 1).


DOI: 10.1021/sc5007347
ACS Sustainable Chem. Eng. 2015, 3, 325−333

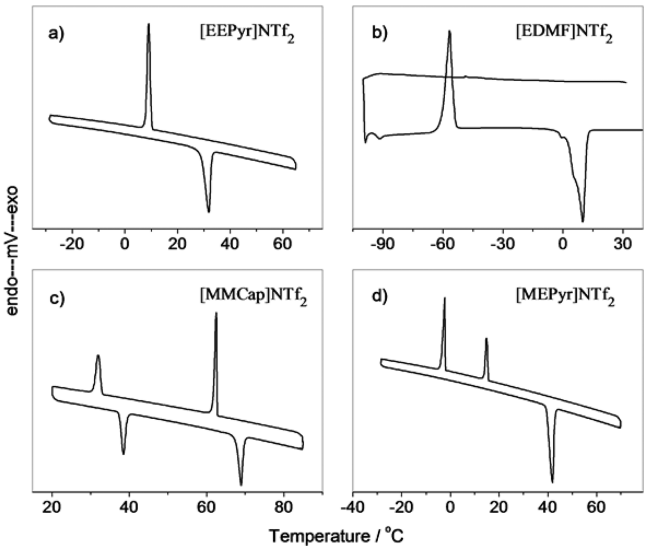


**Figure 2.** Four different types of DSC curves.

For example, [EDEA]TfO underwent a significant enthalpy gain (−35.7 J $g^{-1}$) at 28.1 °C before melting at 48.5 °C. The plastic crystal between two solid states implies their potential application as thermal energy storage materials or solid electrolytes.[48,49] The two different solid states should be related to the existence of two coconformations of $NTf_2$ anion.[50,51] For the fourth type, the solid-plastic crystal transition could be observed upon cooling, but not upon heating (Figure 2d, entries 5, 16, 21, and 24 in Table 1), likely because of the overlapping of two phase transitions upon heating.

All of the ILs were shown to have melting points ($T_m$) less than 100 °C, and four of them melt below 25 °C (entries 1, 2, 9, and 14 in Table 1). Additionally, many of the amidium ILs can remain in a supercooled liquid state at room temperature, with crystallization temperatures ($T_c$) less than 25 °C. For a given anion, the DMF-derived ILs exhibit the lower melting points than the others, including DMA derivatives. DMA could be structurally regarded as C2-methylated DMF, and the structural relationship between DMF and DMA is similar to that of imidazole and C2-methylated imidazole, which are the precursors of a kind of common ILs. For imidazolium ILs, the C2-methylation plays an unexpected role in increasing both melting point and viscosity, contrary to the loss of the predominant hydrogen-bonding interaction between the imidazolium ring C2-H and anion.[52−54] Similar unexpected results could also be observed for the DMF and DMA derived ILs. Although the "acidic" C2-H in DMF ILs increases the interaction between cations and anions via hydrogen bonding, their melting points are much lower than the hydrogen bond-free DMA ILs, e.g., [EDMF]TfO (−32.5 °C) vs [EDMA]TfO (77.0 °C). The possible reason will be discussed in the section of viscosity. Meanwhile, the alkyl groups (methyl vs ethyl) exert a significant but highly variable influence on the melting point. The maximum difference in melting point between the *O*-methylated and *O*-ethylated ILs is 55.7 °C: [MDMF]TfO (23.2 °C) vs [EDMF]TfO (−32.5 °C), in which the replacement of methyl with ethyl clearly decreases melting point. This case accounts for most of the amidium ILs. However, the opposite case also exists, e.g., [MDMA]TfO (42.5 °C) vs [EDMA]TfO (77.0 °C), where the replacement of methyl with ethyl significantly increases melting point. For the case of [EDMF]-TfO and [MDMF]TfO, the reason should be related to the higher flexibility of ethyl group, resulting in packing frustrations, compared with methyl group. While for the case of [EDMA]TfO and [MDMA]TfO, the flexibility of ethyl group is restricted by the C2-$CH_3$ unit, as mentioned in the section of viscosity, and perhaps therefore the melting point of [EDMA]TfO increases even higher than [MDMA]TfO. The impact of anion species (TfO vs $NTf_2$) on melting point is also highly variable, and it is difficult to predict which anion is more likely to cause a low melting point, for instance, [EDMA]TfO (77.0 °C) and [EDMA]$NTf_2$ (33.1 °C) vs [EDMF]TfO (−32.5 °C) and [EDMF]$NTf_2$ (2.9 °C). The high variability of the melting point with its influence factors implies a great degree of interior complexity in the amidium ILs.

The thermal stability of the amidium ILs was investigated by thermogravimetric analysis (TGA), as depicted in Figure 3. The

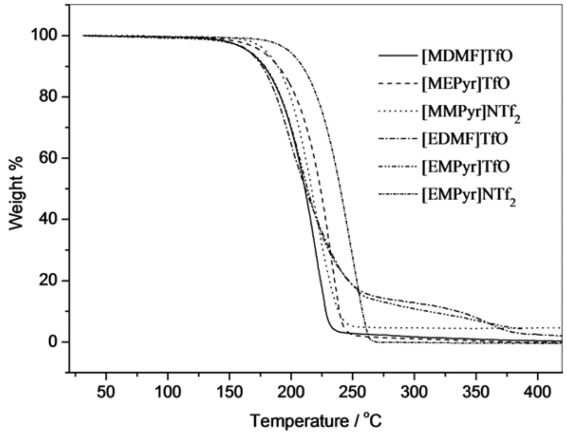


**Figure 3.** TGA curves of six amidium ILs.

resulting thermal decomposition temperature ($T_d$) was recorded at 5% weight loss, and the $T_d$ values fall within the range of 164−204 °C, as listed in Table 1. For a constant cation, $NTf_2$-based amidium ILs are a bit more thermally stable than TfO-based ILs, for example, [EDMF]$NTf_2$ (196 °C) vs [EDMF]TfO (165 °C). Meanwhile, the thermal stability is not significantly impacted by the cationic species, as well as the *O*-alkyl groups. However, the decomposition pattern of TfO-based ILs strongly depends on the *O*-alkyl groups. As shown in Figure 3, with increasing temperature, the mass weight of the *O*-methyl amidium ILs lost gradually until ∼0%; while the *O*-ethyl ILs went through an inflection point at about 20 wt % remnants, and then lost to ∼0%. The inflection in the TGA curves of the *O*-ethylated amidium ILs might be related to the easy formation of protonated amidium during the *O*-ethyl elimination.

For the ILs that are liquids or supercooled liquids at room temperature, their density ($\rho$), surface tension ($\gamma$), viscosity ($\eta$) and its activation energy ($\Delta H_\eta$), conductivity ($\kappa$), and electrochemical stability ($E_{cathodic}$, $E_{anodic}$ and EW) were investigated, and the results are summarized in Table 2. The density of the studied ILs varies in the range of 1.3165−1.5405 g $cm^{-3}$ at 25 °C, close to that of [EMIm]-based ILs. As expected, the $NTf_2$-based ILs are all denser than the TfO-based ILs, because of the more abundant "heavy" elements (S, F, and O) in the former anion. Lengthening the low-density *O*-alkyl chain from methyl to ethyl slightly decreases the density by about 0.06 g $cm^{-3}$. The obtained surface tensions are within the


DOI: 10.1021/sc5007347
ACS Sustainable Chem. Eng. 2015, 3, 325−333

range of 34.5−41.3 mN $m^{-1}$ at 25 °C. In general, the amidium ILs exhibit a bit smaller surface tension than the [EMIm]-based ILs, for example, [EDMF]TfO (35.8 mN $m^{-1}$) vs [EMIm]TfO (41.9 mN $m^{-1}$). Recent evidence indicates that surface tension is intrinsically linked with viscosity, and generally, the smaller surface tension an IL has, the less viscous it will be.[55,56]

The viscosities ($\eta$) of the ILs at 25 and 50 °C are presented in Table 2, ranging 21.6−85.1 cP and 10.2−58.5 cP, respectively. Accordingly, the amidium ILs are preferable to be low-viscosity, in particular, the DMF derivatives. For example, at 25 °C, the viscosity of [EDMF]TfO is only 22.4 cP, which is almost half of that of [EMIm]TfO (43.6 cP). As can be observed, the viscosity values are generally affected by three main factors: (1) amide precursor, (2) *O*-alkyl chain length, and (3) anion species. Keeping the others constant, the viscosity of the amidium ILs increases in the following order: DMF < EPyr < MPyr ≈ DMA < DEA < MCap. In comparison with the other ILs, DMF-derived ILs always possess the lowest viscosity, e.g., [EDMF]$NTf_2$ (21.6 cP) vs [EDMA]$NTf_2$ (40.8 cP) at 25 °C. This result of the DMF ILs, as well as their lowest melting point as stated above, are unexpected and contrary to the presence of hydrogen bond between the "acidic" proton in $N^+$═CH—O moiety and anions. This unexpected phenomenon was also observed in imidazolium ILs, where the C2-methyl group in the imidazolium ring restrains the flexible freedom of its adjacent alkyl chains, leading to an increase in chain-packing efficiency and a decrease in free volume.[52−54] The structural and functional characteristics of the C2-proton in the *O*-alkylated DMF cation are similar to the imidazolium C2-proton. Furthermore, the former was found to follow the same mechanism as the latter. By comparison of [EDMA]-$NTf_2$and [EDMF]$NTf_2$, as described in Table 3, the

**Table 3. Contribution of the $CH_2$ unit [$N^+$═C($CH_3$)—O vs $N^+$═C(H)—O] at Amidium C2 Position to Molar Volume**

| IL | $\rho^a$ (g $cm^{-3}$) | MW$^b$ (g $mol^{-1}$) | MV$^c$ ($cm^3$ $mol^{-1}$) | $\Delta$MV$^d$ ($cm^3$ $mol^{-1}$) |
|---|---|---|---|---|
| [EDMF]$NTf_2$ | 1.4946 | 382.30 | 255.79 | 14.04 |
| [EDMA]$NTf_2$ | 1.4688 | 396.33 | 269.83 | |

[a]Density at 25.0 °C. [b]Molecular weight. [c]Molar volume at 25.0 °C. [d]The difference in molar volume between [EDMA]$NTf_2$ and [EDMF]$NTf_2$ at 25.0 °C.

contribution of the $CH_2$ unit ($CH_3$—H) at the C2 position of the [EDMA] cation to molar volume was calculated to be 14.04 $cm^3$ $mol^{-1}$, much lesser than the normal value of ∼16.7 $cm^3$ $mol^{-1}$.[57−59] The less excess volume could be related to the decrease in flexibility and free volume in the DMA-based ILs, with the resulting increase in melting point and viscosity, compared with the DMF ILs. In other words, the small-sized C2-H in the DMF ILs preserves the side chain flexibility and leads to low melting point and viscosity. In our recent work,[59] this mechanism was proposed to account for the effect of C2-$CH_3$ on imidazolium ILs. Also, in the above order, EPyr-based ILs are much more viscous than their DEA-based counterparts, for example, [EDEA]$NTf_2$ (54.9 cP) vs [EEPyr]$NTf_2$ (33.7 cP) at 25 °C, although EPyr is a cyclic derivative of DEA and they are almost isoelectronic. This result might be related to the asymmetry caused by cyclization, like pyrrolidinium ILs.[60] As can be expected,[61] when the cyclic amide was changed from five-membered MPyr to seven-membered MCap, viscosity would increase dramatically, e.g., [EMPyr]TfO (22.9 cP) vs [EMCap]TfO (58.5 cP) at 50 °C.

The anion species also play an important role in determining the viscosity. For a constant anion, most of the TfO-based ILs are much more viscous than the $NTf_2$ ILs, e.g., at 25 °C [MEPyr]TfO (85.1 cP) vs [MEPyr]$NTf_2$ (46.2 cP), as expected.[62] However, an exception exists with regard to the DMF-derived ILs, and the TfO-based DMF ILs are nearly as low in viscosity as the $NTf_2$ ILs, e.g., [EDMF]TfO (22.4 cP) vs [EDMF]$NTf_2$ (21.6 cP) at 25 °C. Moreover, this exceptional result is also reflected in the following conductivity values.

The *O*-alkylation of the amide carbonyl group brings about the presence of an ether functional group. Ether groups are well-known for their ability to enhance the liquid fluidity, because the highly flexible ether chains cannot pack as efficiently as alkyl chains.[63−65] The presence of ether groups should be an important factor responsible for the low viscosities of the amidium ILs. For the *O*-methylated and *O*-ethylated counterparts, the latter are always less viscous than the former, for example, [EDMF]$NTf_2$ (21.6 cP) vs [MDMF]$NTf_2$ (29.3 cP) at 25 °C, although the ethyl group is bulkier and expected to cause higher viscosity than the methyl group.[66] This unexpected result can be related to the fact that the *O*-terminal rod-like $CH_2CH_3$ tail is more efficient in rotational flexibility than the spherical $CH_3$ tail.[64,65] A similar unexpected result could also be observed for *N*-alkyl groups in the amidium ILs. For example, the amidium ILs containing *N*-ethyl are less viscous than their counterparts containing *N*-methyl, e.g., [EEPyr]$NTf_2$(14.6 cP) vs [EMPyr]$NTf_2$ (16.7 cP) at 50 °C. However, the effect of the replacement of methyl with ethyl on decreasing viscosity in the *O*-alkyl case is dominant over that in the *N*-alkyl case. As a result, for the isomers of [EMPyr]TfO and [MEPyr]TfO, the former (22.9 cP) is less viscous than the latter (29.5 cP) at 50 °C.

The viscosity temperature dependence of the amidium ILs was determined from 25 to 80 °C. As typically shown in Figure4, the viscosity of the ILs decreases exponentially with temperature and follows an Arrhenius-type behavior:

$$(\ln \eta = \ln A + E_\eta/RT)$$

where $\eta$ is viscosity (cP), $A$ is a constant, $E_\eta$ is activation energy (kJ $mol^{-1}$), $R$ is the universal gas constant (8.314 $JK^{-1}$ $mol^{-1}$),

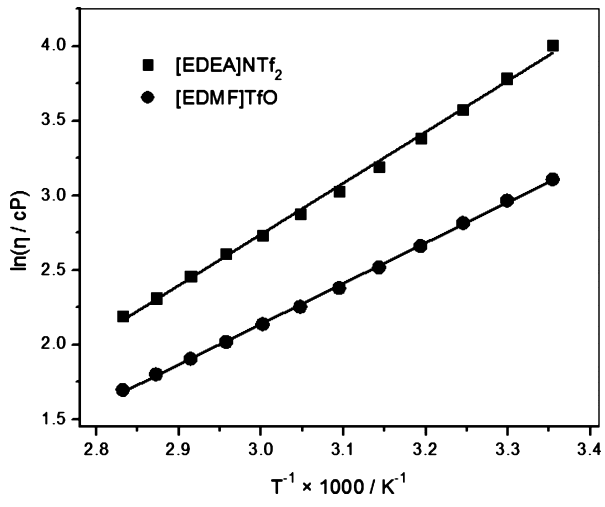


**Figure 4.** Typical Arrhenius plots of viscosity for two amidium ILs.


DOI: 10.1021/sc5007347
ACS Sustainable Chem. Eng. 2015, 3, 325−333

and $T$ is the absolute temperature (K). On the basis of the equation, the activation energy ($E_\eta$) of the viscous ILs was calculated and summarized in Table 2, with the linear fitting parameters ($R^2$) larger than 0.995. In theory, the $E_\eta$ value appears as the energy barrier that needs to be overcome by mass transfer in viscous flow.[67] As a consequence, the more viscous an IL is, the larger $E_\eta$ value it will have. For instance, among these ILs, the least viscous [EDMF]$NTf_2$ (21.6 cP) exhibits the lowest $E_\eta$ value of 21.53 kJ $mol^{-1}$, even in comparison with [EMIm]$NTf_2$ (32.0 cP and 24.42 kJ$mol^{-1}$) at 25 °C.

The conductivity ($\kappa$) of the amidium ILs was measured and presented in Table 2. Generally, the amidium ILs are characterized by high conductivity, with the $\kappa$ values ranging up to 3.48−15.45 mS $cm^{-1}$ at 25 °C. Theoretically, the high conductivity should be correlated with low viscosity.[68] For example, [EDMF]TfO (14.46 mS $cm^{-1}$) is about 1.5 times more conductive than [EMIm]$NTf_2$ (9.27 mS $cm^{-1}$) at 25 °C, while the former (22.4 cP) is only half as viscous as the latter (43.6 cP). With regard to the amide precursors, the conductivity decreases in the order of DMF > DMA > EPyr > DEA, generally contrary to the above-stated viscosity order, except DMA. Another major factor in determining conductivity is ionic sizes, of which the small ones are convenient for mass transfer.[68] The above exception should be attributed to the smaller size of DMA than that of EPyr. Although the replacement of methyl with ethyl at the carbonyl O position always exerts a decreasing effect on viscosity, the related effect on conductivity is uncertain, since the effect of the increased *O*-alkyl chain length on conductivity may compensate and even overcome that of the decreased viscosity. For example, [MDMF]TfO (29.7 cP, 15.45 mS $cm^{-1}$) is more viscous but also more conductive than [EDMF]TfO (22.4 cP, 14.46 mS $cm^{-1}$) at 25 °C. The impact of anion size on conductivity is indeterminate. In most cases, TfO-based ILs are a bit more conductive than $NTf_2$-based ones, although the former are much more viscous than the latter, for example, [EEPyr]TfO (52.3 cP, 6.15 mS $cm^{-1}$) vs [EEPyr]$NTf_2$ (33.7 cP, 6.10 mS $cm^{-1}$). For the DMF derivatives, TfO-based DMF ILs are nearly as low in viscosity as, but smaller in size than $NTf_2$-based ILs, and thus the former are significantly more conductive than latter, e.g., [MDMF]TfO (29.7 cP, 15.45 mS $cm^{-1}$) vs [MDMF]$NTf_2$ (29.3 cP, 10.96 mS $cm^{-1}$) at 25 °C.

A wide electrochemical window is highly desirable for ILs to be applied in electrochemical devices. The electrochemical stability of the amidium ILs was investigated by cyclic voltammetry (CV) on a glassy-carbon electrode, as shown in Figure5. Table 2 lists the resulting values for the cathodic ($E_{cathodic}$) and anodic ($E_{anodic}$) limits, respectively, as well as, the electrochemical windows (EW = $E_{anodic} - E_{cathodic}$). Evidently, all of the amidium ILs have a relatively wide electrochemical window, ranging up to ~4.5 V, which is much wider than the protic amidium ILs (~2.2 V),[34] and comparable to [EMIm]-based ILs (~4.5 V, Table 2). In comparison with [EMIm]-based ILs with $E_{anodic}$ of ~2.3 V, the anodic limit (related to the oxidation of anions) of the amidium ILs is more positive (~2.8 V). Meanwhile, the cathodic limit (related to the reduction of cations) of the latter ($E_{cathodic}$ ~ −1.7 V) is less negative than the former (~−2.2 V). As a result, the overall electrochemical window of the amidium ILs is numerically equal to that of [EMIm] ILs. This difference in anodic limit for the same anion (TfO or $NTf_2$) between the amidium and imidazolium ILs poses the argument that the anion and cation may have a significant influence on each other with respect to the electrochemical stability, although it was generally assumed that the cathodic limit is set by the reduction of the cations and the anodic limit is set by the oxidation of the anions.[69] The cathodic limit of DMF-derived ILs is a bit less negative (~−1.6 V) than other amidium ILs (~−1.8 V). This result should be related to the "acidic" H in the $N^+$═CH—O fragment, similar to imidazolium ILs.[70] All in all, the relatively wide electrochemical window and high conductivity of the amidium ILs indicate their potential application in electrochemistry.

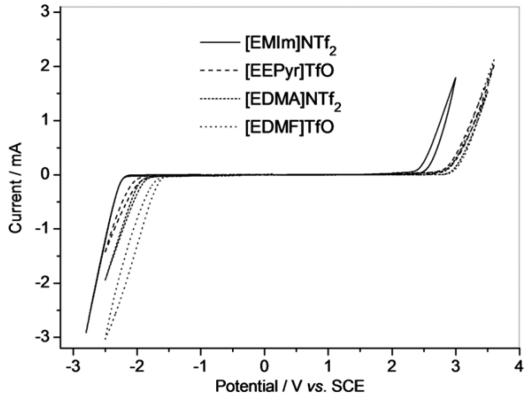


**Figure 5.** Four typical cyclic voltammetry curves of ILs.

## CONCLUSIONS

In conclusion, we synthesized a new class of ILs derived from the low cost (cyclic) amides, via a facile and high-yield approach. Unlike traditional ILs, the amide-derived ILs were formed by the alkylation of the amides with alkyl triflates on the carbonyl oxygen atom, instead of the amide nitrogen atom. As a result of *O*-alkylation, the amidium cations are structurally characterized by (quasi-)planar geometry, low symmetry, and ether moiety, as well as C2-proton in the case of DMF derivatives. These structural characteristics enable the amidium ILs to have high fluidity, especially for the DMF-derived ones. For example, [EDMF]TfO (22.4 cP and 14.46 ms $cm^{-1}$) is even far less viscous and much more conductive than [EMIm]TfO (43.6 cP and 9.27 ms $cm^{-1}$) at 25 °C. The amidium ILs also have relatively wide electrochemical windows up to ~4.5 V, comparable to imidazolium-based ILs, indicating their potential application as nonvolatile electrolytes. Besides, the amidium ILs are ready to form plastic crystals for potential application as thermal energy storage materials or solid electrolytes.

## EXPERIMENTAL SECTION

**Materials.** All commercially available chemicals and solvents were reagent grade quality and used as received without any further purification.

**Synthesis of TfO-based ILs.** The TfO-based amidium ILs were prepared via the *O*-alkylation of amides with alkyl triflates. In a typical procedure, 0.15 mol (11.8 mL) DMF and 60 mL of anhydrous ethyl acetate were placed in a round-bottom flask fitted with a calcium chloride drying tube, and equimolar $CF_3SO_3CH_3$ (17.2 mL) was added dropwise into the mixture at room temperature. After the solution stirred for 20 h at room temperature, diethyl ether and ethyl acetate were added alternately and in small batches to the mixture to form a saturated solution (~250 mL), because the product is miscible with ethyl acetate but not with diethyl ether. The saturated solution was kept at 0 °C until complete crystallization of product, and then the supernatant liquid was decanted. After recrystallization and con-


DOI: 10.1021/sc5007347
ACS Sustainable Chem. Eng. 2015, 3, 325−333

sequent vacuum concentration, 34.5 g of colorless liquid [MDMF]TfO was afforded in 95% yield.

**Synthesis of $NTf_2$-based ILs.** The $NTf_2$-based ILs were synthesized from TfO ILs through anion exchange of TfO with $NTf_2$. In a typical experiment, 0.055 mol $LiNTf_2$ (15.8 g) was added into 30 mL aqueous solution of 0.05 mol [MDMF]TfO (11.9 g), and the solution was stirred for 4 h at 5 °C. During stirring, a white solid precipitated. The solid was vacuum filtrated, washed with 100 mL of distilled water (5 °C), and then vacuum concentrated. 17.3 g of white solid [MDMF]$NTf_2$ was obtained in 94% yield.

**Property Testing.** Before each test, ILs would be vacuum-dried for 20 h at 70 °C and $10^{-3}$ mbar. The solid−liquid phase transition was investigated by using a Mettler-Toledo differential scanning calorimeter model DSC822e, upon a cooling and heating cycle at a scanning rate of 5 °C $min^{-1}$. The thermal stability was measured on a Pyris Diamond PerkinElmer TG/DTA at a rate of 10 °C $min^{-1}$ under $N_2$ atmosphere, and the thermal decomposition temperature was defined as the temperature where 5% weight loss takes place. The density (g $cm^{-3}$) at 25 °C was investigated on a DMA 35 portable density meter, which was calibrated with ultrapure water (0.997 04 g $cm^{-3}$ at 25 °C) and within standard deviation of <0.0002 g $cm^{-3}$. The viscosity (cP) was recorded on a BROOKFIELD DV-II+ Pro viscometer with standard deviation less than 1 cP, inside a glovebox with moisture concentrations below 1 ppm. The surface tension (mN $m^{-1}$) was measured by a Kibron EZ-Pi plus Tensiometer using Wilhemly technique (±0.05 mN $m^{-1}$) at 25 °C. The conductivity (mS $cm^{-1}$) was measured at 25 °C, by a Mettler-Toledo FiveGoTM conductivity meter (±0.05 mS $cm^{-1}$). For the measurement of electrochemical window, the cyclic voltammetry was carried out on a CHI 660D electrochemical workstation with a glassy carbon working electrode, Pt counter electrode and SCE reference electrode. The temperature for the measurements was maintained at ±0.1 °C by means of an external temperature controller, if necessary.

**NMR Data.** The structures of the prepared compounds were confirmed by $^1H/^{13}C$ NMR spectra (ppm, $\delta$) on a BRUKER NMR spectrometer (300 MHz), with TMS as an internal reference in $CD_3CN$, $CDCl_3$, or DMSO-$d_6$. The NMR results including chemical shift, multiplicity, and the number of protons in each signal were presented as follows. The quartet in brackets is assigned to the $^{13}C$ signal of $CF_3$ group in anions.

**[MDMF]TfO.** $^1H/^{13}C$ NMR ($CD_3CN$, 300 MHz, ppm): 8.27 (s, 1H), 4.31 (s, 3H), 3.31 (s, 3H), 3.14 (s, 3H); 167.78, (127.36, 123.12, 118.87, 114.63), 64.60, 41.04, 35.84.

**[MDMF]$NTf_2$.** $^1H/^{13}C$ NMR ($CD_3CN$, 300 MHz, ppm): 8.15 (s, 1H), 4.29 (s, 3H), 3.30 (s, 3H), 3.14 (s, 3H); 167.27, (126.01, 121.76, 117.51, 113.26), 64.39, 40.79, 35.64.

**[EDMF]TfO.** $^1H/^{13}C$ NMR ($CD_3CN$, 300 MHz, ppm): 8.35 (s, 1H), 4.66 (q, 2H), 3.32 (s, 3H), 3.14 (s, 3H), 1.44 (t, 3H); 166.84, (127.41, 123.16, 118.92, 114.67), 75.49, 41.04, 35.83, 14.20.

**[EDMF]$NTf_2$.** $^1H/^{13}C$ NMR ($CDCl_3$, 300 MHz, ppm): 8.38 (s, 1H), 4.74 (q, 2H), 3.41 (s, 3H), 3.23 (s, 3H), 1.51 (t, 3H); 166.71, (126.12, 121.87, 117.62, 113.36), 76.31, 41.71, 36.42, 14.66.

**[MDMA]TfO.** $^1H/^{13}C$ NMR ($CD_3CN$, 300 MHz, ppm): 4.16 (s, 3H), 3.31 (s, 3H), 3.18 (s, 3H), 2.43 (s, 3H); 176.29, (126.92, 122.67, 118.42, 114.17), 59.96, 40.51, 37.98, 13.96.

**[MDMA]$NTf_2$.** $^1H/^{13}C$ NMR ($CD_3CN$, 300 MHz, ppm): 4.15 (s, 3H), 3.30 (s, 3H), 3.18 (s, 3H), 2.42 (s, 3H); 176.25, (126.01, 121.76, 117.52, 113.27), 60.27, 40.79, 38.27, 14.20.

**[EDMA]TfO.** $^1H/^{13}C$ NMR ($CD_3CN$, 300 MHz, ppm): 4.50 (q, 2H), 3.30 (s, 3H), 3.19 (s, 3H), 2.43 (s, 3H), 1.42 (t, 3H); 175.73, (127.48, 123.23, 118.98, 114.73), 70.97, 40.83, 38.50, 14.87, 13.58.

**[EDMA]$NTf_2$.** $^1H/^{13}C$ NMR ($CDCl_3$, 300 MHz, ppm): 4.47 (q, 2H), 3.31 (s, 3H), 3.19 (s, 3H), 2.44 (s, 3H), 1.41 (t, 3H); 175.58, (126.20, 121.94, 117.69, 113.42), 71.39, 41.29, 39.11, 15.15, 14.03.

**[MDEA]TfO.** $^1H/^{13}C$ NMR ($CD_3CN$, 300 MHz, ppm): 4.15 (s, 3H), 3.64 (q, 2H), 3.59 (q, 2H), 2.45 (s, 3H), 1.27 (t, 3H), 1.21 (t, 3H); 175.90, (127.21, 122.96, 118.71, 114.46), 60.04, 46.97, 44.90, 14.20, 11.52, 10.75.

**[MDEA]$NTf_2$.** $^1H/^{13}C$ NMR (DMSO, 300 MHz, ppm): 4.18 (s, 3H), 3.70 (q, 2H), 3.57 (q, 2H), 2.55 (s, 3H), 1.22 (t, 3H), 1.18 (t, 3H); 176.38, (125.87, 121.60, 117.33, 113.07), 60.41, 46.68, 44.49, 14.64, 12.45, 11.68.

**[EDEA]TfO.** $^1H/^{13}C$ NMR ($CD_3CN$, 300 MHz, ppm): 4.50 (q, 2H), 3.62 (m, 4H), 2.45 (s, 3H), 1.42 (t, 3H), 1.27 (t, 3H), 1.22 (t, 3H); 175.26, (127.49, 123.24, 118.99, 114.74), 70.73, 47.06, 45.16, 14.81, 13.47, 11.80, 11.02.

**[EDEA]$NTf_2$.** $^1H/^{13}C$ NMR ($CDCl_3$, 300 MHz, ppm): 4.58 (q, 2H), 3.65 (m, 4H), 2.55 (s, 3H), 1.49 (t, 3H), 1.36 (t, 3H), 1.29 (t, 3H); 175.09, (126.21, 121.95, 117.70, 113.44), 71.26, 47.51, 45.67, 15.05, 14.01, 12.37, 11.66.

**[MMPyr]TfO.** $^1H/^{13}C$ NMR ($CD_3CN$, 300 MHz, ppm): 4.21 (s, 3H), 3.83 (t, 2H), 3.06 (m, 5H), 2.24 (m, 2H); 180.21, (126.93, 122.68, 118.43, 114.18), 61.89, 53.84, 31.51, 28.42, 16.35.

**[MMPyr]$NTf_2$.** $^1H/^{13}C$ NMR ($CDCl_3$, 300 MHz, ppm): 4.21 (s, 3H), 3.85 (t, 2H), 3.11 (m, 5H), 2.29 (m, 2H); 180.18, (126.20, 121.94, 117.69, 113.43), 62.54, 54.61, 32.64, 28.95, 16.87.

**[EMPyr]TfO.** $^1H/^{13}C$ NMR ($CD_3CN$, 300 MHz, ppm): 4.54 (q, 2H), 3.81 (t, 2H), 3.06 (m, 5H), 2.24 (m, 2H), 1.43 (t, 3H); 179.12, (127.18, 122.93, 118.68, 114.43), 72.93, 53.77, 31.74, 28.85, 16.75, 13.50.

**[EMPyr]$NTf_2$.** $^1H/^{13}C$ NMR ($CDCl_3$, 300 MHz, ppm): 4.57 (q, 2H), 3.90 (t, 2H), 3.16 (m, 5H), 2.35 (m, 2H), 1.50 (t, 3H); 179.20, (126.21, 121.95, 117.69, 113.44), 73.10, 53.96, 31.96, 28.99, 16.72, 13.98.

**[MEPyr]TfO.** $^1H/^{13}C$ NMR ($CD_3CN$, 300 MHz, ppm): 4.21 (s, 3H), 3.85 (t, 2H), 3.48 (q, 2H), 3.08 (t, 2H), 2.24 (m, 2H), 1.21 (t, 3H); 179.74, (127.21, 122.96, 118.71, 114.46), 62.12, 51.54, 40.64, 29.00, 16.59, 10.12.

**[MEPyr]$NTf_2$.** $^1H/^{13}C$ NMR ($CDCl_3$, 300 MHz, ppm): 4.28 (s, 3H), 3.91 (t, 2H), 3.57 (q, 2H), 3.21 (t, 2H), 2.38 (m, 2H), 1.28 (t, 3H); 179.83, (126.20, 121.94, 117.68, 113.43), 62.49, 51.85, 41.32, 29.17, 16.75, 10.98.

**[EEPyr]TfO.** $^1H/^{13}C$ NMR ($CD_3CN$, 300 MHz, ppm): 4.54 (q, 2H), 3.83 (t, 2H), 3.52 (q, 2H), 3.07 (t, 2H), 2.24 (m, 2H), 1.43 (t, 3H), 1.21 (t, 3H); 179.07, (127.48, 123.23, 118.98, 114.73), 73.17, 51.50, 40.87, 29.43, 16.99, 13.74, 10.40.

**[EEPyr]$NTf_2$.** $^1H/^{13}C$ NMR ($CDCl_3$, 300 MHz, ppm): 4.59 (q, 2H), 3.90 (t, 2H), 3.57 (q, 2H), 3.20 (t, 2H), 2.35 (m, 2H), 1.50 (t, 3H), 1.28 (t, 3H); 178.96, (126.21, 121.96, 117.70, 113.44), 73.44, 51.51, 41.25, 29.41, 16.90, 14.21, 11.00.

**[MMCap]TfO.** $^1H/^{13}C$ NMR ($CD_3CN$, 300 MHz, ppm): 4.18 (s, 3H), 3.77 (m, 2H), 3.22 (s, 3H), 2.96 (t, 2H), 1.84 (m, 2H), 1.74 (m, 4H); 180.85, (127.48, 123.23, 118.98, 114.73), 60.59, 55.12, 38.90, 28.24, 26.77, 23.98, 20.27.

**[MMCap]$NTf_2$.** $^1H/^{13}C$ NMR ($CDCl_3$, 300 MHz, ppm): 4.26 (s, 3H), 3.83 (t, 2H), 3.31 (s, 3H), 3.04 (t, 2H), 1.90 (m, 2H), 1.81 (m, 4H); 180.87, (126.23, 121.97, 117.71, 113.46), 60.77, 55.69, 39.57, 28.74, 27.05, 24.30, 20.62.

**[EMCap]TfO.** $^1H/^{13}C$ NMR ($CD_3CN$, 300 MHz, ppm): 4.53 (t, 2H), 3.76 (m, 2H), 3.22 (s, 3H), 2.95 (m, 2H), 1.84 (m, 2H), 1.75 (m, 4H), 1.42 (t, 3H); 179.64, (126.93, 122.68, 118.43, 114.17), 70.52, 54.40, 38.30, 27.73, 26.72, 23.45, 19.92, 13.28.

**[EMCap]$NTf_2$.** $^1H/^{13}C$ NMR ($CDCl_3$, 300 MHz, ppm): 4.58 (t, 2H), 3.82 (m, 2H), 3.31 (s, 3H), 3.02 (m, 2H), 1.89 (m, 2H), 1.81 (m, 4H), 1.50 (t, 3H); 180.27, (126.24, 121.98, 117.73, 113.46), 71.45, 55.51, 39.48, 28.77, 27.61, 24.32, 20.86, 14.28.

**[$H^+$EPyr]TfO.** $^1H$ NMR (DMSO, 300 MHz, ppm): 11.18 (s, 1H), 3.33 (t, 2H), 3.19 (q, 2H), 2.21 (t, 2H), 1.92 (m, 2H), 1.01 (t, 3H); $^{13}C$ NMR ($CD_3CN$, 300 MHz, ppm): 177.57, (126.67, 122.44, 118.21, 113.98), 50.40, 39.92, 30.30, 16.73, 10.32.

## AUTHOR INFORMATION


### Corresponding Author

*J.-M. Lee. E-mail: jmlee@ntu.edu.sg. Fax: +65 67947553.


### Notes

The authors declare no competing financial interest.



DOI: 10.1021/sc5007347
ACS Sustainable Chem. Eng. 2015, 3, 325−333

## ■ ACKNOWLEDGMENTS

This work is supported by Academic Research Fund (RGT27/13) of Ministry of Education in Singapore.

## ■ REFERENCES

(1) Cevasco, G.; Chiappe, C. Are ionic liquids a proper solution to current environmental challenges? *Green Chem.* **2014**, *16*, 2375−2385.
(2) Zhang, S. G.; Shi, R.; Ma, X. Y.; Lu, L. J.; He, Y. D.; Zhang, X. H.; Wang, Y. T.; Deng, Y. Q. Intrinsic electric fields in ionic liquids determined by vibrational stark effect spectroscopy and molecular dynamics simulation. *Chem.—Eur. J.* **2012**, *18*, 11904−11908.
(3) Rogers, R. D.; Seddon, K. R. Ionic liquids - Solvents of the future? *Science* **2003**, *302*, 792−793.
(4) Rehman, A.; Zeng, X. Q. Ionic liquids as green solvents and electrolytes for robust chemical sensor development. *Acc. Chem. Res.* **2012**, *45*, 1667−1677.
(5) Hallett, J. P.; Welton, T. Room-temperature ionic liquids: Solvents for synthesis and catalysis. 2. *Chem. Rev.* **2011**, *111*, 3508−3576.
(6) Yu, D. H.; Wang, C. M.; Yin, Y. N.; Zhang, A. J.; Gao, G.; Fang, X. X. A synergistic effect of microwave irradiation and ionic liquids on enzyme-catalyzed biodiesel production. *Green Chem.* **2011**, *13*, 1869−1875.
(7) Ressmann, A. K.; Strassl, K.; Gaertner, P.; Zhao, B.; Greiner, L.; Bica, K. New aspects for biomass processing with ionic liquids: Towards the isolation of pharmaceutically active betulin. *Green Chem.* **2012**, *14*, 940−944.
(8) Yang, D. Z.; Hou, M. Q.; Ning, H.; Ma, J.; Kang, X. C.; Zhang, J. L.; Han, B. X. Reversible capture of $SO_2$ through functionalized ionic liquids. *ChemSusChem* **2013**, *6*, 1191−1195.
(9) Fechler, N.; Fellinger, T. P.; Antonietti, M. "Salt templating": A simple and sustainable pathway toward highly porous functional carbons from ionic liquids. *Adv. Mater.* **2013**, *25*, 75−79.
(10) Tunckol, M.; Durand, J.; Serp, P. Carbon nanomaterial-ionic liquid hybrids. *Carbon* **2012**, *50*, 4303−4334.
(11) Wishart, J. F. Energy applications of ionic liquids. *Energy Environ. Sci.* **2009**, *2*, 956−961.
(12) Macfarlane, D. R.; Forsyth, M.; Howlett, P. C.; Pringle, J. M.; Sun, J.; Annat, G.; Neil, W.; Izgorodina, E. I. Ionic liquids in electrochemical devices and processes: Managing interfacial electrochemistry. *Acc. Chem. Res.* **2007**, *40*, 1165−1173.
(13) Sun, X. Q.; Luo, H. M.; Dai, S. Ionic liquids-based extraction: A promising strategy for the advanced nuclear fuel cycle. *Chem. Rev.* **2012**, *112*, 2100−2128.
(14) Zhang, Y. Q.; Shreeve, J. M. Dicyanoborate-based ionic liquids as hypergolic fluids. *Angew. Chem., Int. Ed.* **2011**, *50*, 935−937.
(15) Zhou, F.; Liang, Y. M.; Liu, W. M. Ionic liquid lubricants: Designed chemistry for engineering applications. *Chem. Soc. Rev.* **2009**, *38*, 2590−2599.
(16) Brown, P.; Butts, C. P.; Eastoe, J.; Hernandez, E. P.; Machado, F. L. D.; de Oliveira, R. J. Dication magnetic ionic liquids with tuneable heteroanions. *Chem. Commun.* **2013**, *49*, 2765−2767.
(17) Tang, S.; Babai, A.; Mudring, A. V. Europium-based ionic liquids as luminescent soft materials. *Angew. Chem., Int. Ed.* **2008**, *47*, 7631−7634.
(18) Wu, B.; Liu, W.; Zhang, Y.; Wang, H. Do we understand the recyclability of ionic liquids? *Chem.—Eur. J.* **2009**, *15*, 1804−1810.
(19) Dong, K.; Zhao, L. D.; Wang, Q.; Song, Y. T.; Zhang, S. J. Are ionic liquids pairwise in gas phase? A cluster approach and in situ IR study. *Phys. Chem. Chem. Phys.* **2013**, *15*, 6034−6040.
(20) Leal, J. P.; Esperanca, J.; da Piedade, M. E. M.; Lopes, J. N. C.; Rebelo, L. P. N.; Seddon, K. R. The nature of ionic liquids in the gas phase. *J. Phys. Chem. A* **2007**, *111*, 6176−6182.
(21) Vitorino, J.; Leal, J. P.; da Piedade, M. E. M.; Lopes, J. N. C.; Esperanca, J.; Rebelo, L. P. N. The nature of protic ionic liquids in the gas phase revisited: Fourier transform ion cyclotron resonance mass spectrometry study of 1,1,3,3-tetramethylguanidinium chloride. *J. Phys. Chem. B* **2010**, *114*, 8905−8909.
(22) Earle, M. J.; Esperanca, J.; Gilea, M. A.; Lopes, J. N. C.; Rebelo, L. P. N.; Magee, J. W.; Seddon, K. R.; Widegren, J. A. The distillation and volatility of ionic liquids. *Nature* **2006**, *439*, 831−834.
(23) Taylor, A. W.; Lovelock, K. R. J.; Deyko, A.; Licence, P.; Jones, R. G. High vacuum distillation of ionic liquids and separation of ionic liquid mixtures. *Phys. Chem. Chem. Phys.* **2010**, *12*, 1772−1783.
(24) Zhu, X.; Wang, Y.; Li, H. R. Do all the protic ionic liquids exist as molecular aggregates in the gas phase? *Phys. Chem. Chem. Phys.* **2011**, *13*, 17445−17448.
(25) King, A. W. T.; Asikkala, J.; Mutikainen, I.; Jarvi, P.; Kilpelainen, I. Distillable acid-base conjugate ionic liquids for cellulose dissolution and processing. *Angew. Chem., Int. Ed.* **2011**, *50*, 6301−6305.
(26) Li, Z.; Li, C. P.; Chi, Y. S.; Wang, A. L.; Zhang, Z. D.; Li, H. X.; Liu, Q. S.; Welz-Biermann, U. Extraction process of dibenzothiophene with new distillable amine-based protic ionic liquids. *Energy Fuels* **2012**, *26*, 3723−3727.
(27) Berg, R. W.; Lopes, J. N. C.; Ferreira, R.; Rebelo, L. P. N.; Seddon, K. R.; Tomaszowska, A. A. Raman spectroscopic study of the vapor phase of l-methylimidazolium ethanoate, a protic ionic liquid. *J. Phys. Chem. A* **2010**, *114*, 10834−10841.
(28) Choi, N. S.; Chen, Z. H.; Freunberger, S. A.; Ji, X. L.; Sun, Y. K.; Amine, K.; Yushin, G.; Nazar, L. F.; Cho, J.; Bruce, P. G. Challenges facing lithium batteries and electrical double-layer capacitors. *Angew. Chem., Int. Ed.* **2012**, *51*, 9994−10024.
(29) Zhang, Q. H.; Vigier, K. D.; Royer, S.; Jerome, F. Deep eutectic solvents: Syntheses, properties and applications. *Chem. Soc. Rev.* **2012**, *41*, 7108−7146.
(30) Abbott, A. P.; Capper, G.; Davies, D. L.; Rasheed, R. K.; Tambyrajah, V. Novel solvent properties of choline chloride/urea mixtures. *Chem. Commun.* **2003**, 70−71.
(31) Deng, D. S.; Cui, Y. H.; Chen, D.; Ai, N. Solubility of $CO_2$ in amide-based Bronsted acidic ionic liquids. *J. Chem. Thermodyn.* **2013**, *57*, 355−359.
(32) Palgunadi, J.; Im, J.; Kang, J. E.; Kim, H. S.; Cheong, M. $CO_2$ solubilities in amide-based Bronsted acidic ionic liquids. *Bull. Korean Chem. Soc.* **2010**, *31*, 146−150.
(33) Xiang, J.; Chen, R. J.; Wu, F.; Li, L.; Chen, S.; Zou, Q. Q. Physicochemical properties of new amide-based protic ionic liquids and their use as materials for anhydrous proton conductors. *Electrochim. Acta* **2011**, *56*, 7503−7509.
(34) Du, Z. Y.; Li, Z. P.; Guo, S.; Zhang, J.; Zhu, L. Y.; Deng, Y. Q. Investigation of physicochemical properties of lactam-based Bronsted acidic ionic liquids. *J. Phys. Chem. B* **2005**, *109*, 19542−19546.
(35) Huang, J. F.; Baker, G. A.; Luo, H. M.; Hong, K. L.; Li, Q. F.; Bjerrum, N. J.; Dai, S. Bronsted acidic room temperature ionic liquids derived from N,N-dimethylformamide and similar protophilic amides. *Green Chem.* **2006**, *8*, 599−602.
(36) Xu, F.; Chen, H. Y.; Zhang, H. B.; Zhou, X. H.; Cheng, G. Z. Protophilic amide ionic liquid assisted esterification and catalysis mechanism. *J. Mol. Catal. A: Chem.* **2009**, *307*, 9−12.
(37) Lee, J. S.; Mayes, R. T.; Luo, H. M.; Dai, S. Ionothermal carbonization of sugars in a protic ionic liquid under ambient conditions. *Carbon* **2010**, *48*, 3364−3368.
(38) Luo, H. M.; Huang, J. F.; Dai, S. Solvent extraction of $Sr^{2+}$ and $Cs^{+}$ using protic amide-based ionic liquids. *Sep. Sci. Technol.* **2010**, *45*, 1679−1688.
(39) Demberelnyamba, D.; Shin, B. K.; Lee, H. Ionic liquids based on N-vinyl-gamma-butyrolactam: Potential liquid electrolytes and green solvents. *Chem. Commun.* **2002**, 1538−1539.
(40) Yang, J.; Zhang, Q. H.; Zhu, L. Y.; Zhang, S. G.; Li, J.; Zhang, X. P.; Deng, Y. Q. Novel ionic liquid crystals based on N-alkylcaprolactam as cations. *Chem. Mater.* **2007**, *19*, 2544−2550.
(41) Burrell, A. K.; Del Sesto, R. E.; Baker, S. N.; McCleskey, T. M.; Baker, G. A. The large scale synthesis of pure imidazolium and pyrrolidinium ionic liquids. *Green Chem.* **2007**, *9*, 449−454.
(42) Wasserman, H. H. Chemistry - Synthesis with a twist. *Nature* **2006**, *441*, 699−700.


DOI: 10.1021/sc5007347
*ACS Sustainable Chem. Eng.* 2015, 3, 325−333

(43) Meerwein, H.; Borner, P.; Fuchs, O.; Sasse, H. J.; Schrodt, H.; Spille, J. Reaktionen mit Alkylkationen. *Chem. Ber.* **1956**, *89*, 2060−2079.
(44) Meerwein, H.; Florian, W.; Schön, N.; Stopp, G. Über Säureamidacetale, Harnstoffacetale und lactamacetale. *Justus Liebigs Ann. Chem.* **1961**, *641*, 1−39.
(45) Wanzlick, H. W.; Kleiner, H. J. Nucleophile carben-chemie darstellung des Bis-[1.3-diphenyl-imidazolidinyliden-(2)]. *Angew. Chem.* **1961**, *73*, 493−493.
(46) Bredereck, H.; Effenberger, F.; Simchen, G. Säureamid-Reaktionen, XXXII. Über säureamid-dialkylsulfat-komplexe. *Chem. Ber.* **1963**, *96*, 1350−1355.
(47) Chen, Z. J.; Xi, H. W.; Lim, K. H.; Lee, J. M. Distillable ionic liquids: Reversible amide O alkylation. *Angew. Chem., Int. Ed.* **2013**, *52*, 13392−13396.
(48) Armel, V.; Velayutham, D.; Sun, J. Z.; Howlett, P. C.; Forsyth, M.; MacFarlane, D. R.; Pringle, J. M. Ionic liquids and organic ionic plastic crystals utilizing small phosphonium cations. *J. Mater. Chem.* **2011**, *21*, 7640−7650.
(49) Janikowski, J.; Razali, M. R.; Batten, S. R.; MacFarlane, D. R.; Pringle, J. M. Organic ionic plastic crystals and low viscosity ionic liquids based on the dicyano(nitroso)methanide anion. *ChemPlusChem* **2012**, *77*, 1039−1045.
(50) Holbrey, J. D.; Reichert, W. M.; Rogers, R. D. Crystal structures of imidazolium bis(trifluoromethanesulfonyl)imide "ionic liquid" salts: The first organic salt with a cis-TFSI anion conformation. *Dalton Trans.* **2004**, 2267−2271.
(51) Martinelli, A.; Matic, A.; Johansson, P.; Jacobsson, P.; Borjesson, L.; Fernicola, A.; Panero, S.; Scrosati, B.; Ohno, H. Conformational evolution of $TFSI^-$ in protic and aprotic ionic liquids. *J. Raman Spectrosc.* **2011**, *42*, 522−528.
(52) Peppel, T.; Roth, C.; Fumino, K.; Paschek, D.; Kockerling, M.; Ludwig, R. The influence of hydrogen-bond defects on the properties of ionic liquids. *Angew. Chem., Int. Ed.* **2011**, *50*, 6661−6665.
(53) Izgorodina, E. I.; Maganti, R.; Armel, V.; Dean, P. M.; Pringle, J. M.; Seddon, K. R.; MacFarlane, D. R. Understanding the effect of the C2 proton in promoting low viscosities and high conductivities in imidazolium-based ionic liquids: Part I. Weakly coordinating anions. *J. Phys. Chem. B* **2011**, *115*, 14688−14697.
(54) Zhang, Y.; Maginn, E. J. The effect of C2 substitution on melting point and liquid phase dynamics of imidazolium based-ionic liquids: Insights from molecular dynamics simulations. *Phys. Chem. Chem. Phys.* **2012**, *14*, 12157−12164.
(55) Abbott, A. P. Application of hole theory to the viscosity of ionic and molecular liquids. *ChemPhysChem* **2004**, *5*, 1242−1246.
(56) Zhao, H.; Liang, Z. C.; Li, F. An improved model for the conductivity of room-temperature ionic liquids based on hole theory. *J. Mol. Liq.* **2009**, *149*, 55−59.
(57) Fang, D. W.; Guan, W.; Tong, J.; Wang, Z. W.; Yang, J. Z. Study on physicochemical properties of ionic liquids based on alanine $[C_{(n)}mim][Ala]$ (n=2,3,4,5,6). *J. Phys. Chem. B* **2008**, *112*, 7499−7505.
(58) Glasser, L. Lattice and phase transition thermodynamics of ionic liquids. *Thermochim. Acta* **2004**, *421*, 87−93.
(59) Chen, Z. J.; Lee, J. M. Free volume model for the unexpected effect of C2-methylation on the properties of imidazolium ionic liquids. *J. Phys. Chem. B* **2014**, *118*, 2712−2718.
(60) Baek, B.; Lee, S.; Jung, C. Pyrrolidinium cation-based ionic liquids with different functional groups: Butyl, butyronitrile, pentenyl, and methyl butyrate. *Int. J. Electrochem. Sci.* **2011**, *6*, 6220−6234.
(61) Belhocine, T.; Forsyth, S. A.; Gunaratne, H. Q. N.; Nieuwenhuyzen, M.; Puga, A. V.; Seddon, K. R.; Srinivasan, G.; Whiston, K. New ionic liquids from azepane and 3-methylpiperidine exhibiting wide electrochemical windows. *Green Chem.* **2011**, *13*, 59−63.
(62) Ignat'ev, N. V.; Barthen, P.; Kucheryna, A.; Willner, H.; Sartori, P. A convenient synthesis of triflate anion ionic liquids and their properties. *Molecules* **2012**, *17*, 5319−5338.
(63) Siqueira, L. J. A.; Ribeiro, M. C. C. Alkoxy chain effect on the viscosity of a quaternary ammonium ionic liquid: Molecular dynamics simulations. *J. Phys. Chem. B* **2009**, *113*, 1074−1079.
(64) Zhou, Z. B.; Matsumoto, H.; Tatsumi, K. Low-melting, low-viscous, hydrophobic ionic liquids: N-Alkyl(alkyl ether)-N-methylpyrrolidinium perfluoroethyltrifluoroborate. *Chem. Lett.* **2004**, *33*, 1636−1637.
(65) Chen, Z. J.; Xue, T.; Lee, J. M. What causes the low viscosity of ether-functionalized ionic liquids? Its dependence on the increase of free volume. *RSC Adv.* **2012**, *2*, 10564−10574.
(66) Slattery, J. M.; Daguenet, C.; Dyson, P. J.; Schubert, T. J. S.; Krossing, I. How to predict the physical properties of ionic liquids: A volume-based approach. *Angew. Chem., Int. Ed.* **2007**, *46*, 5384−5388.
(67) Batabyal, S.; Mondol, T.; Pal, S. K. Picosecond-resolved solvent reorganization and energy transfer in biological and model cavities. *Biochimie* **2013**, *95*, 1127−1135.
(68) Bonhote, P.; Dias, A. P.; Papageorgiou, N.; Kalyanasundaram, K.; Gratzel, M. Hydrophobic, highly conductive ambient-temperature molten salts. *Inorg. Chem.* **1996**, *35*, 1168−1178.
(69) Ong, S. P.; Andreussi, O.; Wu, Y. B.; Marzari, N.; Ceder, G. Electrochemical windows of room-temperature ionic liquids from molecular dynamics and density functional theory calculations. *Chem. Mater.* **2011**, *23*, 2979−2986.
(70) Hapiot, P.; Lagrost, C. Electrochemical reactivity in room-temperature ionic liquids. *Chem. Rev.* **2008**, *108*, 2238−2264.


DOI: 10.1021/sc5007347
*ACS Sustainable Chem. Eng.* 2015, 3, 325−333